Calibration of the first XMM Flight Mirror Module II - Effective Area

Ph. Gondoin[a], B. Aschenbach[b], M. Beijersbergen[a], R. Egger[b]
F. Jansen[a], Y. Stockman[c], J.P. Tock[c]

[a] European Space Research and Technology Center, 2200 AG Noordwijk zh, the Netherlands

[b] Max-Planck Institute fur Extraterrestrische Physik, 8046 Garching, Germany

[c] Centre Spatial de Liege, B-4031 Liege, Belgium

ABSTRACT

The High Throughput X-ray Spectroscopy Mission (XMM) is a "Cornerstone" Project in the ESA long-term Programme for Space Science. The satellite observatory uses three grazing incidence mirror modules coupled to reflection grating spectrometers and X-ray CCD cameras. Each XMM mirror module consists of 58 Wolter I mirrors which are nested in a coaxial and cofocal configuration. The calibration of the mirror system includes the development of a representative numerical model and its validation against extensive calibration tests performed on ground at the CSL and PANTER test facilities. The present paper describes the calibration of the x-ray effective area of the first XMM flight mirror module.

Keywords: XMM, X-ray astronomy, Wolter I telescope, grazing incidence optics

1. INTRODUCTION

The X-ray Multi-Mirror Observatory XMM[1] is a "Cornerstone" project in the ESA long-term programme for space science due for launch in August 1999. The primary scientific objective of XMM is to perform high throughput spectroscopy of cosmic x-ray sources over a broad band of energies ranging from 0.1 keV to 10 keV. The XMM model payload includes:

- three grazing incidence mirror modules[2,3],
- three CCD imaging cameras (EPIC)[4,5] one at the prime focus of each mirror module, which provide imaging in a 30 arcmin field of view and broadband spectroscopy with a resolving power of between 5 and 60 in the energy band 0.1 to 10 keV,
- two reflection grating spectrometers (RGS)[6] which provide spectroscopy between 0.1 and 3 keV with a resolving power of over 250 at 0.5 keV,
- one optical monitor (OM)[7] which permits simultaneous monitoring of x-ray sources in the optical and UV spectral range.

With the spectroscopic capability of the mirror modules associated to the EPIC and RGS instruments (see Figure 1), XMM will improve our understanding of hot astrophysical plasma. The interpretation of this next generation data requires that calibration of the telescopes and payload is performed to a high level of accuracy. For instance, in order to derive the differential emission measure distribution of optical thin plasma as a function of temperature, as well as for deriving elemental abundance, we need to know relative line intensities and the continuum to an accuracy of 5 to 10 percent. Thus the accuracy on the mirror module effective area and encircled energy function at all energy should be 2 - 3 percent throughout the 0.1 to 10 keV passband.

The absence of cosmic x-ray sources which could serve as in-orbit calibration standards prevents an in orbit calibration of the mirror modules to a high level of accuracy. The effective area and encircled energy function of the mirrors have therefore to be calibrated on ground. The situation is further complicated since on-ground testing cannot be performed in fully representative operation conditions. Indeed, full aperture X-ray test data gathered

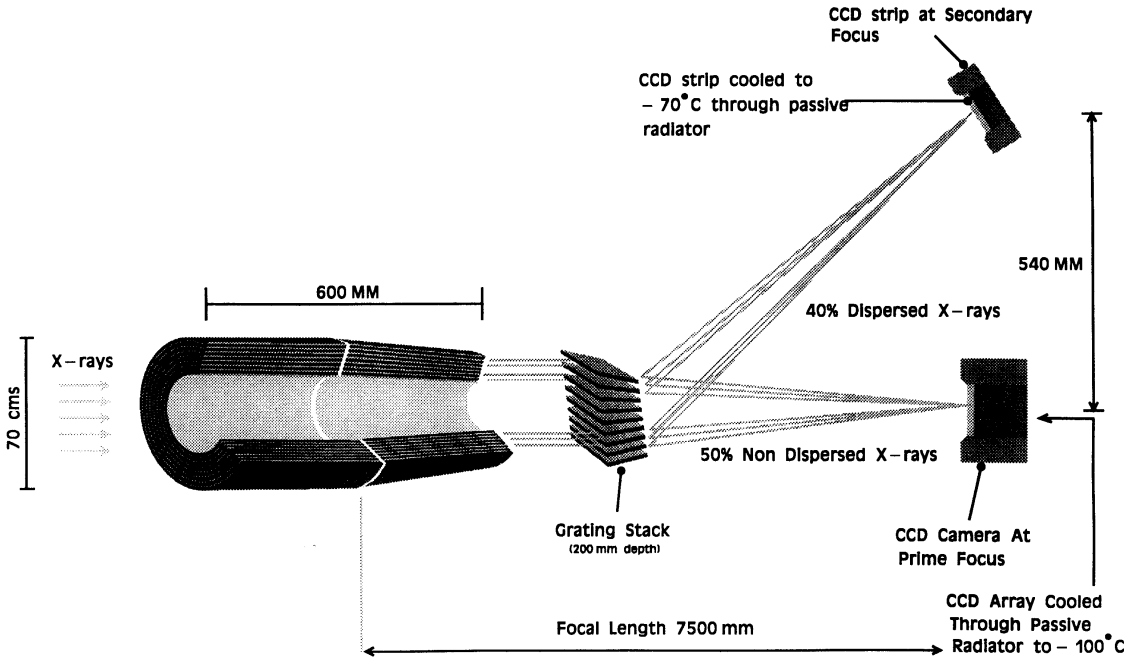

Figure 1. optical layout of an XMM mirror module combined with the RGS and EPIC experiments

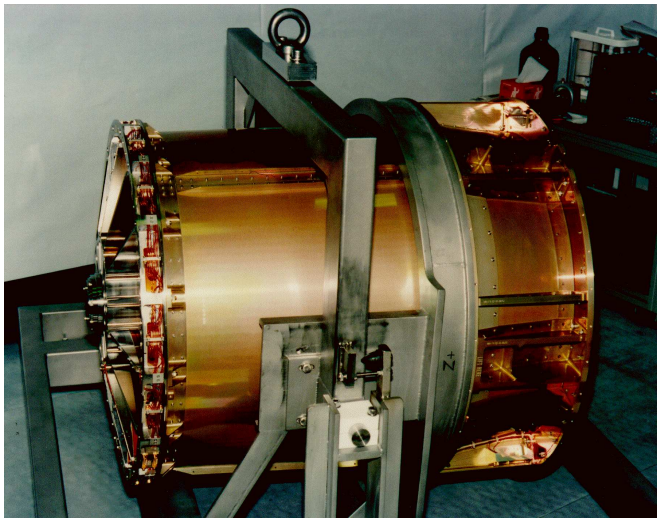

Figure 2. XMM FM1 mirror module without x-ray baffles

at the MPE long beam Panter Facility is compromised by the finite source distance. In such tests a large fraction of the reflecting surfaces of the mirror shells are not used. Full aperture data for a source at infinity is available from the CSL vertical test facility but only at EUV wavelengths. In order to overcome these difficulties and to satisfy the calibration requirements, a comprehensive and reliable numerical model of the XMM mirror system has been built[2]. This model simulates the reflection efficiency of the mirrors and the vignetting effect of the incident beam by the mirror module structure which includes the entrance x-ray baffles, the sixteen spokes spider, the mirror nest and the exit magnetic deflector. The effective collecting area of the mirror module is calculated by ray-tracing

incident photons through this numerical model taking into account the figuring errors and surface roughness of the mirrors. Each individual ray carries an intensity coefficient which account for scattering and reflectivity losses. The gold surface reflectivity is calculated from tables of refraction indices using the Fresnel equation for a semi-infinite medium. In the x-ray range above 100 eV, the 1993 Henke table[8] is used initially as updated by Gullikson based on new absorption coefficient data to improve the description of the gold M absorption edge. Below 100 eV, we used the refraction index table from D.W. Lynch and W.R. Hunter[9]. Calibrating the effective area of the XMM mirror modules consists in validating this numerical model based on the results of on-ground x-ray pencil beam and full aperture illumination tests. This is performed in successive steps. First the mirror reflectivity function is determined by x-ray pencil beam tests. Then the on-axis vignetting effect of the mirror entrance spider and exit magnetic deflector are measured by on-axis partial and full aperture x-ray tests. Finally, after integration of the front x-ray baffle, the off-axis vignetting function and the straylight rejection efficiency of the mirror module are characterized in a EUV collimated beam. The present paper describes these different calibration steps performed on the first XMM flight mirror module.

2. MIRROR REFLECTIVITY MEASUREMENTS

The CSL vertical test facility[10] provides a vertical x-ray channel which can be used to perform pencil beam tests on any single mirror of an integrated XMM mirror module. An x-ray pencil beam test was performed on 15 of the 58 mirrors of the first flight module both at 1.5 keV and 8.0 keV. These include the 10 smallest mirrors with diameters ranging from 303 mm to 345 mm, the largest 700 mm diameter mirror and four intermediate size mirrors. For each mirror, the intensity of the beam reflected successively on the parabola and hyperbola section was measured at two azimuths using a solid state detector. The intensity ratio R_{meas} of this double reflected beam to the direct beam was calculated. Table 1 provides the double reflection efficiency of the ten smallest FM1 mirror shells which have very similar grazing angles. For a pencil beam parallel to the optical axis, the grazing angle is identical on the parabola and hyperbola section and ranges between 17 and 20 arcmin for the ten smallest XMM mirrors. The reflection efficiency data provided in table 1 are the average values of pencil beam measurements performed on each mirror at two different azimuths. They are compared with the theoretical values R_{th} calculated from the Henke 93 table of optical constants.

Table 1. measured and theoretical reflection efficiency of the smallest FM1 mirrors

Grazing ang.	1.5 keV		8.0 keV	
(arcmin)	R_{th}	R_{meas}	R_{th}	R_{meas}
19.8	0.86	0.76	0.74	0.59
19.5	0.86	0.84	0.75	0.67
19.3	0.86	0.82	0.75	0.69
19.0	0.87	0.86	0.75	0.68
18.7	0.87	0.86	0.76	0.70
18.4	0.87	0.76	0.76	0.61
18.2	0.87	0.83	0.77	0.69
17.9	0.87	0.79	0.77	0.65
17.6	0.88	0.83	0.78	0.69
17.4	0.88	0.81	0.78	0.64

Table 1 indicates that shells having similar grazing angles exhibit a double reflection efficiency which is in average lower than theory by about 5 and 10 percents respectively at 1.5 keV and 8.0 keV. This can be partly explained as follows. The reflectivity measurements were performed with a solid state detector having a 20 mm diameter entrance window. Angle scatter measurements performed on a single mirror shell[2] having a representative power spectral density show that scattering losses outside a 10 mm radius window amount to 0.2 and 6 percent respectively at 1.5

keV and 8.0 keV. Different roughness of the mirror surfaces partly explain the shell to shell variation in reflection efficiency. However, the average reflection efficiency corrected from scatter losses is still lower than theory by 4 percents both at 1.5 and 8 keV. Hence, for single reflections, the XMM mirror reflectivity is lower than the theoretical value predicted by the Fresnel formulae using the Henke 93 table of optical constants by 2 percents. Therefore, when using the Henke table of optical constants, an empirical correction function to the Fresnel formulae is needed to provide an accurate description of the XMM mirror reflectivity.

Among hundreds of images of the XMM mirror surface obtained with a microscope interferometer, a few reveal the presence of circular signature quite unusual on other mirror images. Also unexplained, these circular features are reminiscent of Airy diffraction pattern which could be expected from unresolved surface peaks or dust particles. In order to estimate the possible effect of dust on mirror reflectivity at 1.5 keV and 8.0 keV, a simple dust contamination model was used[11]. Particles would absorb and diffractively scatter x-rays outside the detector field of view. The effect of dust contamination on a single reflection can therefore be described by the following expression where α is the grazing angle and F_{dust} the fractional dust coverage expressed in ppm.

$$R_{Fdust}(\alpha) = R_0(\alpha).[1 - 2.Q_{a,s}.Fdust/(10^6.sin(\alpha))]$$

The factor of 2 in the above formula accounts for the vignetting by a spherical dust particle of both the incident and reflected beam. We assume that the absorption and scattering efficiency $Q_{a,s}$ of the dust particles is unity. In practice some scattered photons could still reach the detector. Figure 3 provides the reflectivity measurements point of 15 of the 58 XMM mirrors at two azimuths. The figure illustrates how the Fresnel equation using the Henke-Gullikson optical constant is successively affected by scattering losses, dust contamination and reduced density of the reflectivity coating with respect to bulk gold density. A reduced density of the gold coating only modifies the mirror reflectivity close to the critical angle and does not effect the XMM mirror reflectivity at low energy. A good fit to both the 1.5 keV and 8.0 keV measured reflectivity curve is achieved assuming a 100 ppm surface vignetting. The reflectivity model described above was implemented in the ray-tracing code to interpolate between energy and grazing angle since it provides a reasonable fit to the reflectivity measurement points. The reflectivity correction function could have been more accurately tuned as a function of energy and grazing angle if reflection efficiency had been measured on all mirror shells at a larger number of energies. This will be performed during the calibration campaign of the FM2, FM3 and FM4 mirror modules using five different x-ray energies distributed over the XMM spectral range.

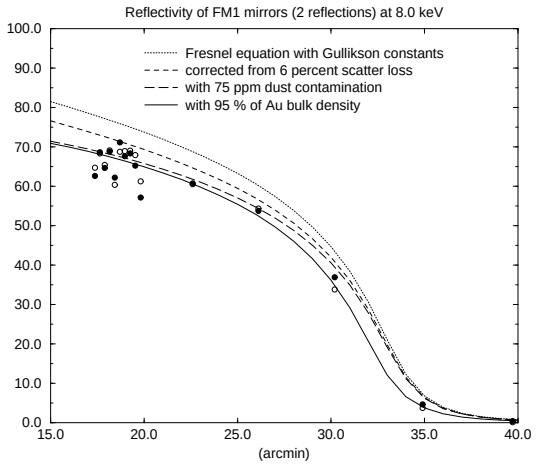

Figure 3. reflectivity of FM1 mirrors at 8 keV

3. X-RAY MEASUREMENTS OF THE ON-AXIS EFFECTIVE AREA

3.1. Full aperture tests with finite source distance

After environmental and EUV test at CSL, the XMM mirror modules are sent to the PANTER facility[12] for x-ray calibration under vacuum. The facility consists of a source chamber and an instrument test chamber connected by a tube of 130 meter length. The instrument test chamber is 13 meters long and has a diameter of 3.5 meters. It is equipped with an optical bench which hosted the FM1 mirror module. In its image plane, two detectors were mounted on a manipulator. The ROSAT Position Sensitive Proportional Counter (PSPC) was used for effective area measurements of the FM1 mirror module. The PSPC was positioned at a 60 mm intrafocal position to avoid unfavourable obscuration by the wire mesh supporting the PSPC entrance window. Additionaly, the detector was slowly moved hence and forth perpendicularly to the optical axis in order to smear out the image evenly across the entrance window. A reference measurement without the mirror module was performed after each exposure. Brightness stability of the x-ray source was monitored with four proportional counters located near the mirror entrance aperture.

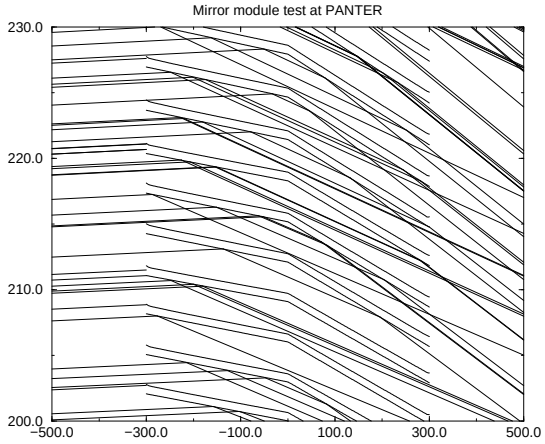

Figure 4. ray propagation of the PANTER divergent beam through XMM mirrors

The calibration tests at PANTER provide a full aperture illumination in x-ray with however some limitations (see Figure 4). Because of the finite source distance, the first ten centimeters of the mirror parabola do not contribute to the image formation by double reflections. In addition, a few millimeters of the mirror surface near the parabola to hyperbola intersection plane is shadowed due to the dense packing geometry of the XMM mirror nest. Finally, the mirrors operate under a higher grazing angle with respect to infinite source distance which significantly reduces their reflectivity at high energy. The effective area of an XMM mirror module is therefore more than 30 percent lower under PANTER illumination condition than under the nominal in-orbit operation condition.

The numerical model of the FM1 mirror module which includes workshop metrology data of the mirror surface and the empirical correction to the theoretical surface reflectivity was used to simulate the PANTER test configuration. Figure 5 compares the simulation results with effective area measurement of the FM1 and FM2 mirror modules performed at twelve different energies. The simulated effective area exceeds by 3 to 4 percent average the measurement points. The deficit is not due to an inaccurate description of the mirror reflectivity which was empirically incorporated in the model from pencil beam measurements. An intra-focal image of the x-ray source by the FM1 mirror module rather suggests a vignetting effect possibly related to the divergence of the input beam. Indeed, the radial energy distribution in the intra-focus image shows a surface brightness reduction with respect to simulation at a radius corresponding to mirror diameters included between 372 mm and 567 mm. Vignetting of medium size shells by their inner neighbour could be responsible of an additional effective area loss which is not accurately simulated by the

model. Table 2 gives the effective area sensitivity to mirror imperfections when the mirror module is tested either in the PANTER convergent beam or in an x-ray parallel beam. The table provides the relative effective area change of a perfect XMM mirror module calculated by the simulator when including in the numerical model the effect of the workshop metrology data. This includes the measured increase of shell thickness at mirror edge, the mirror misalignment, the mirror out of roundness, the mirror surface figuring errors and the mirror reflectivity.

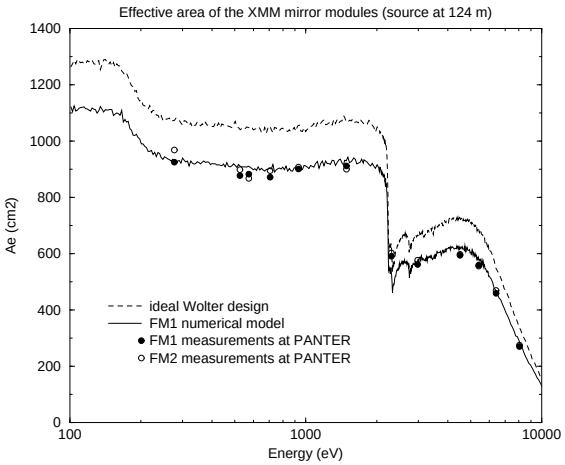

Figure 5. full aperture measurement of the on-axis effective area of the FM1 mirror module at PANTER

Table 2. sensitivity of effective area measurements to mirror imperfections

Mirror defects	Source at infinity δAe/Ae	PANTER configuration δAe/Ae
increase of edge thickness	0.00	0.07
misalignment	0.00	0.02
out of roundness	0.00	0.00
axial figuring errors	0.02	0.00
reflectivity losses	0.06	0.06

Table 2 indicates a slight sensitivity of the effective area measurements to axial profile errors in an infinite source distance configuration. This can be explained as follows. Large slope errors are only present close to the mirror edges and at the parabola to hyperbola intersection plan. These slope errors are large enough to deflect incoming rays outside the detector field of view. Since the first 100 mm of the mirror shells and a few mm of the parabola to hyperbola intersection zone are not probed in the PANTER test configuration, the effective area measurement is not sensitive to profile errors when the source is at a finite distance. Table 2 also indicates that effective area measurements in the infinite source distance configuration is not sensitive to relative decenter between mirrors. Indeed, the XMM mirror packing density was designed such that, in a parallel beam configuration, a significant decenter of a mirror shell with respect to its inner neighbour is needed before shadowing of its parabola section occurs. In the finite source distance configuration, the incoming beam is divergent and the parabola section of one mirror is already slightly shadowed by its closest inner neighbour. A relative decenter of these shells is then sufficient to alter the on-axis effective area.

At infinite source distance, the effective area is mainly determined by the surface reflectivity. Geometrical effects play a minor role. At finite source distance on the contrary, both surface reflectivity losses and vignetting by mirror thicknesses significantly affect the on-axis effective area. An increase of the mirror thickness close to the edges was noticed on XMM mirrors. Indeed, sharp edges locally increase the electrical field in the mirror production bath and induce a higher electro-forming rate at mirror extremities. Thickness measurements of all shells were therefore performed at 5 mm and 10 mm from the entrance aperture and extrapolated linearly to the mirror extremities. The uncertainty associated to this extrapolation explain the 3 to 4 percents discrepancy between the measured and simulated effective area of the XMM mirror module in the PANTER divergent beam.

3.2. Sub-aperture tests with pseudo-infinite source distance

Effective area measurements with an infinite source distance are not possible on ground. However, partial aperture tests with a source positioned on the normal to the sub-aperture mask at mask center simulate with a good accuracy an infinite source distance. Such a set-up was designed[12] to allow a full calibration of the XMM mirror module at PANTER in a quasi-paraxial illumination. It includes a variable aperture mask called Glucksrad positioned in front of the mirror module that allows selective illumination of limited parts of its entrance aperture. The Glucksrad device consists of two independently steel wheels movable around a same axis which is coaligned with the mirror module optical axis. The first wheel contains a sector shaped aperture that fits the sectors defined by the spider spokes supporting the mirrors. The second wheel contains four apertures that enable separate illumination of four radial zones corresponding to the outermost mirrors, the innermost mirrors and two groups of intermediate size mirrors. Appropriate combination of sectors and zones by rotating the wheels allows for a quasi parallel beam illumination of well defined part of the mirror module entrance aperture. At any subaperture position, the optical axis of the mirror module is aligned such that the x-ray source is located on the normal to the subaperture mask at mask center. Thus the radial beam divergence is limited to +/- 40 arc-seconds for the PANTER source distance of 124822 mm. The overall effective area for an infinite source distance can then be measured by co-adding all subaperture tests results. In this configuration, there is no substantial difference with the in-orbit performance. The Glucksrad measurements can therefore be regarded as a direct absolute calibration of the mirror module effective area.

Table 3. measured and simulated effective area of the FM2 mirror module for an infinite source distance

Energy (keV)	FM2 measurements Ae (cm2)	Simulation Ae (cm2)	Sim. acc. (percent)
0.277	1469.3 (+/-2.5)	1467	0.0
1.486	1433.2 (+/-2.3)	1466	+2.3
8.050	617.16 (+/-1.6)	611	-1.0

Glucksrad measurements were performed on the second XMM flight mirror module which behaves similarly to the first model (see Figure 5). The measurement results are compared in Table 3 and Figure 6 with the simulation results of the in-orbit effective area. The simulation used the FM1 numerical model with all metrology data and the reflectivity correction function established from the CSL pencil beam reflectivity tests of individual mirror shells. The simulation accuracy is better than 3 percents at the three measured energies. The Glucksrad tests provide a higher calibration accuracy than the full aperture test with the finite source distance. In the Glucksrad test, the effective area measurement condition are representative of the in-orbit operation conditions and less sensitive to exact geometry of the shells. Increase of the mirror thicknesses close to the entrance aperture does not alter the effective area measurement results. Glucksrad tests have therefore been introduced in the calibration campaign of the FM2, FM3 and FM4 XMM mirror modules. They will be performed with all accessible Glucksrad sub-apertures to these three flight models at 1.5 keV and 8.0 keV. These tests will be complemented by four subaperture measurements along one sector of each mirror module at four additional energies. The combined analysis of these Glucksrad test results will provide an accurate calibration of the absolute effective area of the mirror modules across the XMM spectral range.

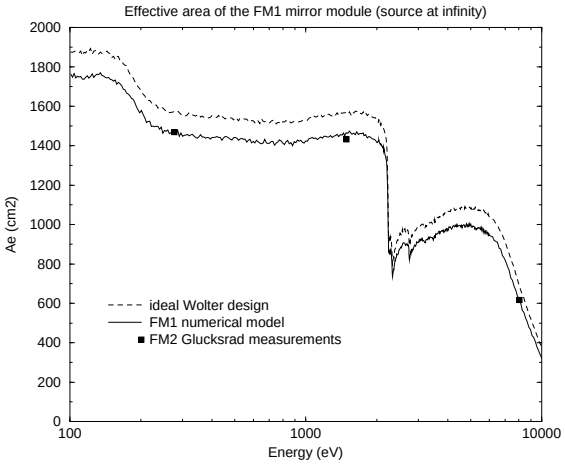

Figure 6. Glucksrad measurements of FM2 effective area at PANTER

4. MEASUREMENT OF THE OFF-AXIS VIGNETTING FUNCTION

4.1. Off-axis x-ray effective area with finite source distance

The off-axis effective area measured in a full aperture illumination at PANTER is given in Figure 7 as a function of the off-axis angles. No significant difference is observed between the measurements performed in two perpendicular azimuthal direction. The data points are compared with effective area simulation in the divergent beam at 1.5 keV, 4.5 keV, 6.4 keV and 8.0 keV. The simulation of the vignetting effect relative to the on-axis effective area is extremely accurate. The few percent offset with respect to the absolute measurements is due to the accuracy limitation inherent to the full aperture configuration.

The full aperture test in the finite source distance configuration induces a unusual off-axis change of the effective area. Indeed, the vignetting function is flat up to 6 arcmin off-axis angles at low energy. At high energy, it even

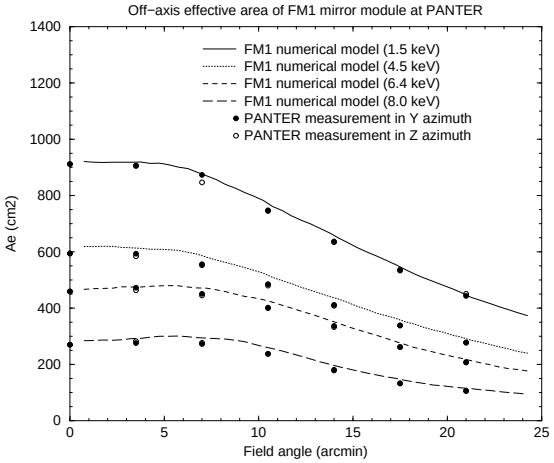

Figure 7. off-axis effective area of FM1 mirror module at PANTER

slightly increases with small off-axis angles. This behaviour is quite different from the expected in-orbit performance. Furthermore the finite source distance precludes measurements of the effective area when the mirror modules are equipped with x-ray baffles. The calibration of the vignetting function of the XMM mirror module requires a collimated beam.

4.2. EUV measurements of the mirror module vignetting function

Full aperture illumination tests are performed at the CSL vertical facility[10] which provides a full aperture vertical collimated beam. An electron cyclotron resonance EUV source which emits in the HeI and HeII lines at 58 and 30 nm illuminates a pinhole placed at the focus of a vertical Cassegrain telescope. The platinium coated primary and secondary mirrors provide a parallel beam of 800 mm diameter. The x-ray mirror module is positioned above the Cassegrain telescope in the vertical collimated beam. It focuses the beam through aluminium filters on a thinned back side illuminated CCD. The overall set-up is located in a vertical vacuum chamber. Effective area measurements were performed on the FM1 mirror module by dividing the count rate recorded in an extra-focal image of the FM1 mirror module by a reference measurements of the input flux. The EUV effective area of the FM1 mirror module was measured on-axis before and after integration of the x-ray baffles. No significant change was detected above the measurement repeatability. The absence of on-axis vignetting of the mirror module by the x-ray baffles was corroborated by comparing intrafocus images and cross aperture pencil beam scans before and after integration of the baffles.

Table 4. vignetting function of the FM1 mirror module

off-axis angle	w/o baffles		with baffles	
(arcmin)	measurements	simulation	measurements	simulation
0	1.00	1.00	1.00	1.00
5	0.87	0.88	0.85	0.80
10	0.66	0.65	0.57	0.53
15	0.46	0.44	0.34	0.33

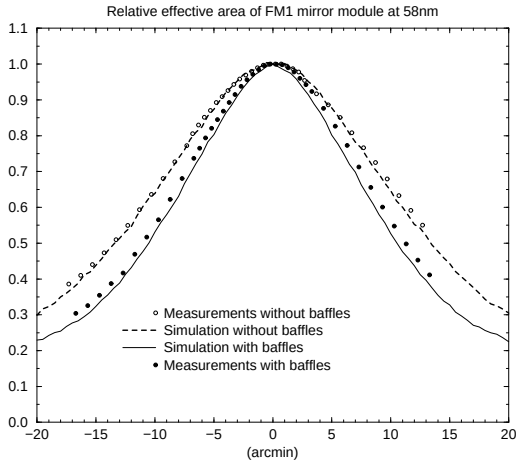

Figure 8. EUV measurements of the FM1 vignetting function with and without x-ray baffle

Off-axis effective area measurements relative to the on-axis value are given in Table 4 before and after integration of the x-ray baffles. The simulation accuracy of the relative off-axis effective area at PANTER demonstrates that this

EUV vignetting function can be confidently extrapolated to the x-ray spectral domain by the mirror simulator. Figure 8 shows the EUV vignetting function of the FM1 mirror module with and without x-ray baffles. The measurement points are compared with simulation results. The simulation match the vignetting function of the mirror module without x-ray baffles to better than 2 percent but underestimates the vignetting effect of the two sieves of the x-ray baffles. Part of this underestimate of the vignetting function arises from the description of the x-ray baffles in the numerical model. Indeed, the model incorporates measured dimension of the fifty eight annular apertures of the two baffle sieves but does not describes the chamfer on the edges of the annular slits. This chamfer was machined to reduced edge diffraction effect in the optical range. It also slightly decreases the vignetting effect by the sieves of a collimated off-axis beam. Correction of the model will be implemented for the FM2, FM3 and FM4 mirror modules but is not expected to fully account for vignetting function underestimate. An alternative explanation is the presence of diffused or diffracted light in the EUV test which has not been simulated since it does not occur in the x-ray domain.

5. STRAYLIGHT TESTS

Without x-ray baffles, the XMM mirror modules suffer from x-ray straylight. The effect is that the image of a 30 arcmin square area of the sky in the EPIC field of view can be contaminated by a diffuse light background produced by x-ray sources located outside this field. EPIC observations of isolated sources and RGS spectra are hardly affected. For extended source on the contrary such as the diffuse x-ray background, supernovae remnants, cluster of galaxies, stellar cluster and star forming regions, there is a severe limitation in the ability to do spatially resolved spectroscopy. X-ray straylight in EPIC is produced by rays which are singly reflected by the mirror hyperbola and which reach unfocussed the sensitive area of the EPIC camera. An x-ray baffle was designed to shadow those single reflected rays. It consists of two sieve plates made of concentric annular aperture stops located in front of the mirrors respectively at 85 mm and 145 mm. The design is such that the entrance annular aperture of each mirror remains unobstructed for on-axis rays. Most of the rays with large off-axis angle are vignetted and cannot reach anymore the EPIC detector via a single hyperbola reflection.

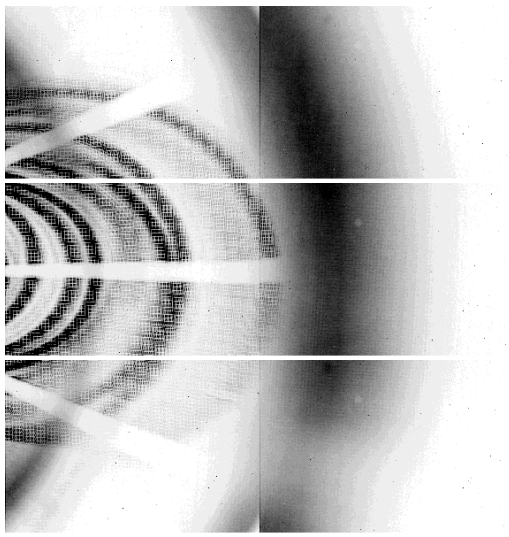

Figure 9. measured EUV straylight distribution in the EPIC field of view from a 30 arcmin off-axis source

Figure 9 shows the measured EUV straylight distribution produced in the EPIC field of view by a source located 30 arcmin off-axis. It was obtained by juxtaposition of 6 CCD images registered at the CSL vertical facility. The image exhibits sharp rings opened towards the paraxial image of the source located outside of the detector field. These sharp rings are produced by single residual reflection on the hyperbola sections of intermediate size mirrors. The fuzzier intensity distribution with a double ring shape seen in Figure 9 is not reproduced by the simulation. Its

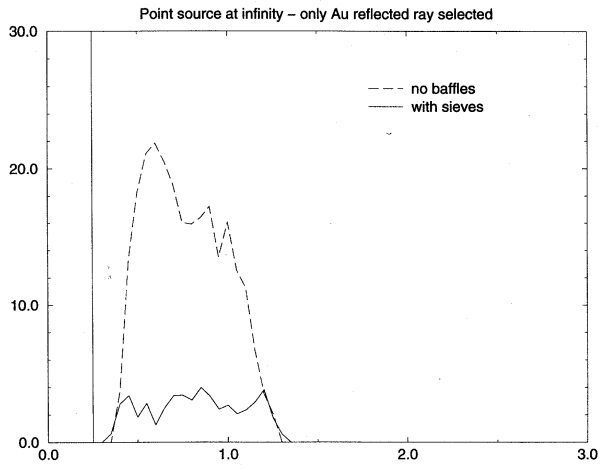

Figure 10. straylight collecting area in the EPIC field of view at 1.5 keV

integrated brightness is lower than the single hyperbola reflection rings. The double ring structure likely originates from grazing incidence reflection on the back nickel surface of intermediate size mirrors. These two stray rings would therefore not be visible in x-rays due to the high surface roughness of the rear nickel mirror surface. This will be confirmed by subaperture straylight tests in x-rays using if possible the Glucksrad device at PANTER. The straylight collecting area in the EPIC detector as a function of the off-axis angle of a point source is anticipated to be as given on Figure 10. The ratio of the x-ray straylight collecting area to the on-axis effective area is smaller than 0.2 percent at 1.5 keV for a point source located at off-axis angle included between 0.4 and 1.4 degree and negligible at higher off-axis angle. This ratio expressed in surface brightness is even smaller since the stray-image is unfocussed at detector position. This illustrates the high straylight rejection efficiency of the XMM mirror modules.

6. CONCLUSIONS

An optimum recipe for the on-ground effective area calibration of the XMM mirror modules has been established. It consists of the following steps.

- pencil beam reflectivity measurements of individual mirrors at various energies distributed along the XMM spectral range,
- development of a numerical model of an XMM mirror module simulating vignetting effect, mirror figuring errors, surface scattering and reflectivity,
- measurements of the on-axis effective area by subaperture illumination of the mirror modules at the PANTER facility
- measurements of the vignetting function of the mirror modules after integration of the x-ray baffles and eventually of the reflection grating assembly using the EUV collimated beam of the CSL vertical facility,
- generation of effective area calibration files by extrapolating on-ground measurements to in-orbit operation condition using the validated software model.

This recipe was applied to the calibration of the first XMM flight mirror module. The simulation accuracy of the EUV and x-ray measurement tests demonstrates that the 3 percent calibration goal of the effective area can be achieved over most of the XMM spectral range with the possible exception of the gold M absorption edge. Integrated system tests combining the XMM mirror modules and the EPIC experiment will focussed on this specific spectral range around 2.2 keV using either a continuum source or energy scans provided by a monochromator.

7. ACKNOWLEDGMENTS

We wish to congratulate the MEDIALARIO mirror manufacturing team for the outstanding performance of the XMM flight mirror modules. Many thanks go to our colleagues from the PANTER and CSL test facilities for their dedication to the calibration tests of the XMM mirror modules.

8. REFERENCES

1 F. Jansen, "XMM Observatory: a scientific and technical overview", These Proceedings.

2 Ph. Gondoin, B. Aschenbach, M. Beijersbergen, R. Egger, F. Jansen, Y. Stockman, J.P. Tock, "Calibration of the first XMM flight mirror module - 1 Image quality", These proceedings.

3 D. de Chambure, R. Laine, "X-ray telescopes for the ESA XMM spacecraft", Thes proceedings.

4 A.D.Holland, M.J.L.Turner, A.F.Abbey, P.J. Pool, "MOS CCDs for the EPIC on XMM", SPIE Proc.2808, pp. 414-420, 1996

5 N. Meidinger, H.W. Brauninger, R. Hartmann, G. Hartner, N. Krause, E. Pfeffermann, C. Reppin, G. Schwaab, L. Struder, J. Trumper, P. Holl, J. Kemmer, S. Krisch, H. Soltau, C. van Zanthier, D. Hauf, R. Richter, "PN-CCD detector for the European Photon Imaging Camera on XMM", SPIE Proc.2808, pp. 492-503, 1996

6 A.C.Brinkman, H.J.M.Aaarts, A.J.F.den Boggende, L.Dubbeldam, J.W.den Herder, J.S.Kaastra, P.A.J.de Korte, R.Mewe, C.J.Hailey, S.M.Kahn, F.B.S.Paerels, G.Branduardi-Raymont, J.V.Bixler, K.Thomsen, A.Zehnder, "Reflection Grating Spectrometer on-board XMM", SPIE Proc.2808, pp. 463-480, 1996

7 R. Much, D. Lumb, M.S. Cropper, R. Hunt, K.O. Mason, F.A. Cordova, T. Sasseen, C. Ho, W. Priedhorsky, C.Jamar, E. Antonello, "The Optival/UV Monitor on the X-ray Multi Mirror Mission",Proceedings of the Conference " Ultraviolet Astrophysics, Beyond the IUE Final Archive", Sevilla, Spain, 11-14 November 1997, ESA SP-413, pp.815, 1998

8 B.L. Henke, E.M Gullikson E.M., J.C Davis, Atomic Data and Nuclear Data Tables, July 1993, Vol 54

9 D.W. Lynch and W.R. Hunter, "Handbook of Optical Constants of Solids", ed. E.D. Palik, Academic Press, Orlando, 1985

10 Y. Stockman, J.P. Tock, D. de Chambure, Ph. Gondoin, "XMM flight mirror module environmental and optical testing", These proceedings.

11 R.F. Elsner, M. Joy, S.L. O'Dell, B.D. Ramsey, M.C. Weisskopf,"Ground-to-orbit transfer of the AXAF-I flux scale - In situ contamination monitoring of x-ray telescopes", SPIE Proc.2279, 1994.

12 R. Egger, B. Aschenbach, H. Brauninger, W. Burket, T. Dohring, A. Oppitz," X-ray calibration of the XMM flight mirror modules at the PANTER test facility", These proceedings.